ELSEVIER

Journal of Alloys and Compounds 454 (2008) 194–200

Journal of ALLOYS AND COMPOUNDS

www.elsevier.com/locate/jallcom

Effect of Y for enhanced age hardening response and mechanical properties of Mg–Ho–Y–Zr alloys

J. Wang [a,b], D.P. Zhang [a], D.Q. Fang [a], H.Y. Lu [a], D.X. Tang [a], J.H. Zhang [a], J. Meng [a,*]

[a] *Key Laboratory of Rare Earth Chemistry and Physics, Changchun Institute of Applied Chemistry, Chinese Academy of Sciences, Changchun 130022, China*

[b] *Graduate School of the Chinese Academy of Science, Beijing 100049, China*

Received 18 October 2006; received in revised form 22 December 2006; accepted 25 December 2006

Available online 7 January 2007

Abstract

In this study, compositional dependence of age hardening characteristics and tensile properties were investigated for Mg–4Ho–*x*Y–0.6Zr alloys ($x = 0$, 3, 5, and 7 wt%). The result showed that with increasing Y content, the hardness of the alloys increased in the as-quenched and aged-peak conditions. Considerable age hardening response was recognized for the alloys. When the alloy containing 7% Y showed the most remarkable age hardening response at aging temperature of 250 °C. The tensile strength of the alloys increased monotonously with increasing Y content, and Mg–4Ho–7Y–0.6Zr exhibited the maximum ultimate tensile strength and yield strength at peak hardness, and the values were 240 and 165 MPa at room temperature, and 204 and 131 MPa at 250 °C, respectively. The improvement in strength appeared to be associated with β′ and/or equilibrium $Mg_{24}Y(Ho)_5$ precipitates and high dense dislocation.

Keywords: Magnesium alloys; Precipitation hardening; Mg–Ho–Y–Zr; Age hardening response

1. Introduction

Lightweight Mg alloys have attracted increasing interest in recent years for potential applications in the aerospace, aircraft and automotive industries due to their high strength/weight ratio [1]. The addition of rare earth (RE) elements remarkably improves the mechanical properties of Mg alloys at room temperature (RT) and high temperature duo to solution hardening and precipitation hardening [2–7]. The beneficial effects of RE additions on the properties such as strength and creep resistance of the cast and wrought magnesium alloys are well known.

Mg–heavy rare earth (RE) alloys (e.g. WE alloys Mg–Y–Nd–Zr, Mg–Gd–Nd–Zr, Mg–Gd–Y, Mg–Gd, etc.) exhibit remarkable ageing hardening by plate-shaped precipitates parallel to all equivalent prismatic planes of α-Mg matrix [8–11]. Over-saturated α-Mg solid solution decomposes according to the following sequence in all of those alloys [12]: α-Mg → β″ (D019) metastable phase → β′ (bco) metastable phase → β (fcc). Rare earth element Ho is also a important element in all heavy rare earth elements. The equilibrium solid solubility of the Ho in Mg relatively high (6.44 at% or 26.08 wt%) at 588 °C and decrease exponentially, with the decrease in temperature, to (2.10 at% or 12.8 wt%) at 200 °C, forming an ideal system for precipitation hardening. It is known that binary Mg–Gd alloys containing less than 10 wt% Gd show little or no precipitation hardening response during isothermal or isochronal ageing of supersaturated solid [11]. Accordingly it is possible that binary Mg–Ho alloys containing low Ho show little or no precipitation hardening response during isothermal or isochronal ageing.

It is the purpose of the present paper to investigate the age hardening response during isothermal ageing at 250 °C of the Mg–4Ho–*x*Y–0.6Zr alloys ($x = 0$, 3, 5, and 7 wt%), and test of tensile properties of these alloys.

2. Experimental procedure

The Mg–Y–Ho–Zr alloys were made by melting Mg–30% Ho, Mg–20% Y, Mg–25% Zr master alloys, pure Mg in a graphite crucible with the protection of potassium chloride. When the temperature reached 750 °C, molten metals were poured into steel mold. Table 1 gives the chemical compositions of the studied alloys in this work. Ingots were solution treated for 10 h at 525 °C quenched into

* Corresponding author. Tel.: +86 431 5262030; fax: +86 431 5698041.
E-mail address: jmeng@ciac.jl.cn (J. Meng).

0925-8388/$ – see front matter © 2007 Elsevier B.V. All rights reserved.
doi:10.1016/j.jallcom.2006.12.120

Table 1
Chemical composition of Mg–Y–Ho–Zr alloys

Nomianal alloy	Composition (wt%)			
	Ho	Y	Zr	Mg
Mg–4Ho–Zr	3.70	0	0.53	Bulk
Mg–4Ho–3Y–Zr	3.69	2.94	0.61	Bulk
Mg–4Ho–5Y–Zr	3.64	4.73	0.58	Bulk
Mg–4Ho–7Y–Zr	3.58	6.56	0.52	Bulk

hot water. The hardness testing of the alloys was taken using Vickers hardness (Hv) tester. Tensile tests were performed at a crosshead speed of 1 mm/min at room temperature and high temperature using Instron-type tensile testing machine. Microstructures of both as-cast and heat treated alloys were observed with an optical microscope and morphologies of secondary phase were observed by transmission electron microscopy (TEM). Tensile fractures were observed using scanning electron microscopy (SEM).

3. Result and discussion

3.1. Microstructure and aging behavior

As-cast microstructure of the studied alloys is showed in Fig. 1(a)–(d). With increasing Y content, the dendritic eutectic of α-Mg solid solution and RE-rich second phase in the triple junction of grain boundaries were formed, and the volume fraction of intermetallic phases increased. In present work, the Mg–4Ho–0.6Zr alloy had relatively coarse grains, typically about 200 μm in diameter, in Fig. 1(a). An addition of Y to 3 wt% in the Mg–4Ho–0.6Zr alloy led to finer grains of α-Mg grain and the average grain size in the alloy was 50 μm in diameter, in Fig. 1(b). A further increase in the Y content from 5 or 7 wt% did not affect the grain size, compared with Mg–4Ho–3Y–0.6Zr alloy, in Fig. 1(c) and (d). It was indicated that Y had a remarkable effect on grain refinement.

The microstructures of solution-treated Mg–4Ho–*x*Y–0.6Zr alloys ($x = 0$, 3, 5, and 7 wt%) were shown in Fig. 2(a)–(d). Almost all the eutectic phases were solutionized into Mg matrix, and the average grain sizes were 250, 150, 70 and 50 μm, respectively. For Mg–4Ho–0.6Zr and Mg–4Ho–3Y–0.6Zr alloys, the grain size was much larger than that of as-cast states. A few intermetallic particles at grain boundaries still remained at and near grain boundaries, as shown in Fig. 2(d). The TEM micrograph for these particles persisted during subsequent age is shown in Fig. 3. The quadrate phase was about 0.4 μm in length, and this morphology is representative in the investigated area. These particles seemed to be $Mg_{24}Y(Ho)_5$ phases of body centered cubic structure.

Fig. 4 compares hardness curves of Mg–4Ho–0.6Zr alloys, with and without systematic Y additions, obtained during isothermal ageing 250 °C. The ternary Mg–4Ho–0.6Zr alloy had a hardness value of 43 Hv in the as-quenched condition, and exhibited little age hardening response during isothermal ageing, with a maximum value of 47 Hv being obtained. When 3 wt% Y was added to the Mg–4Ho–0.6Zr alloy, a substan-

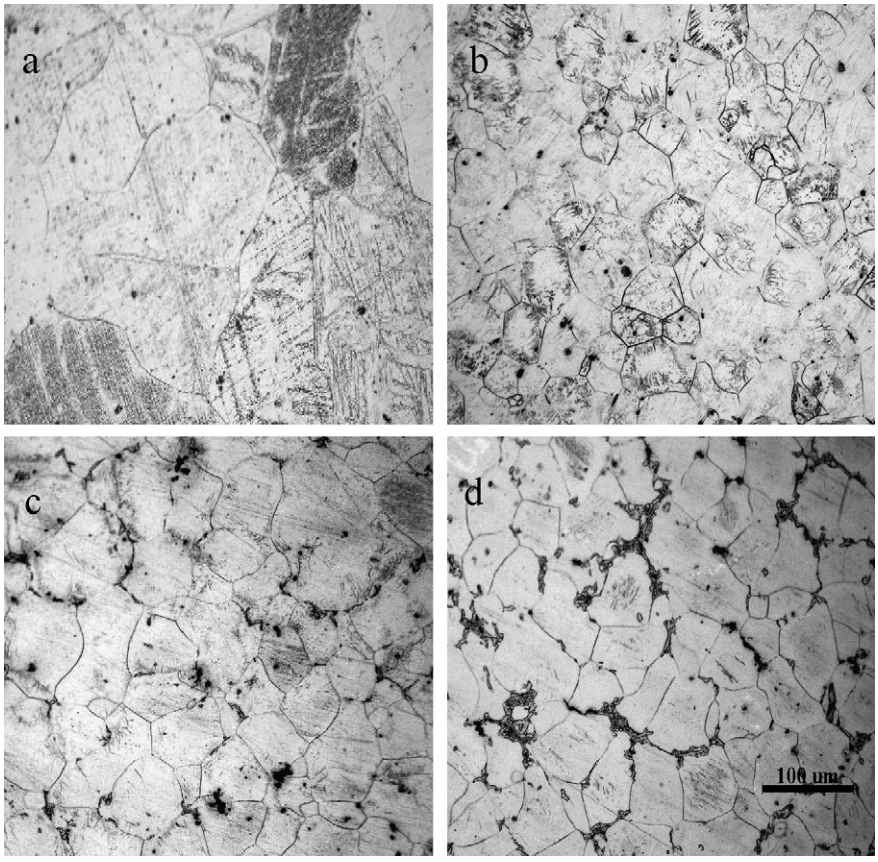

Fig. 1. Optical micrograph of the as-cast Mg–4Ho–*x*Y–0.6Zr alloys: (a) $x = 0$; (b) $x = 3$; (c) $x = 5$; (d) $x = 7$.

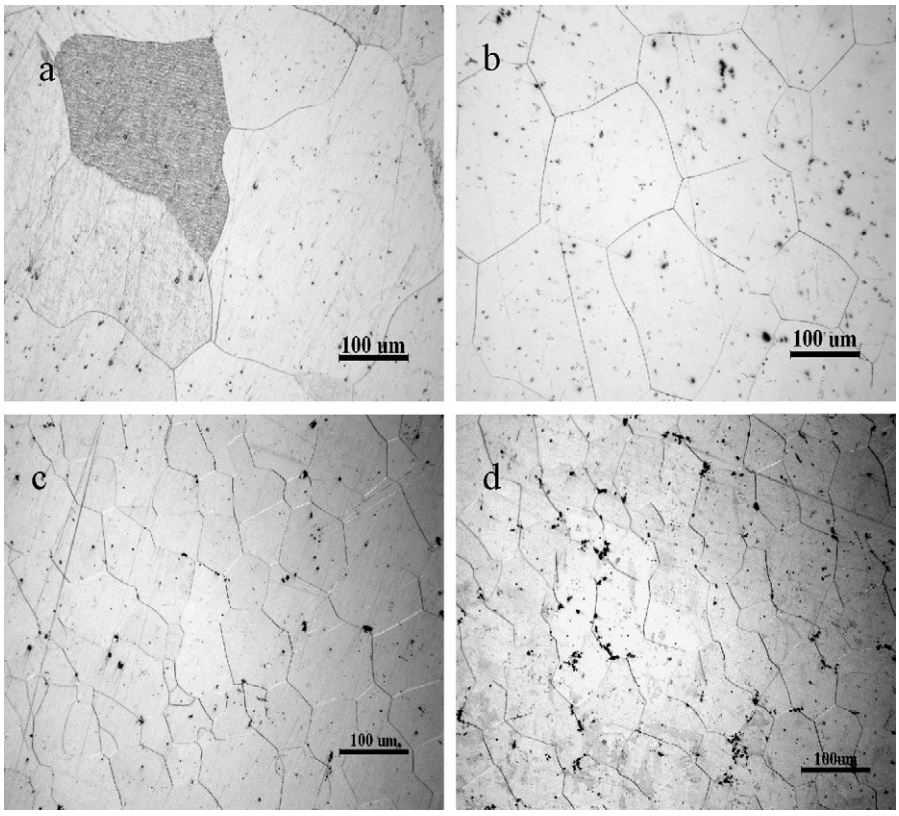

Fig. 2. Optical micrograph of the solution-treated Mg–4Ho–*x*Y–0.6Zr alloys: (a) $x = 0$; (b) $x = 3$; (c) $x = 5$; (d) $x = 7$.

tial increase in hardness was observed in both as-quenched and peak-aged condition. In the as-quenched condition, the Mg–4Ho–3Y–0.6Zr alloy had a hardness value of approximately 69 Hv, which was about 58% higher than that of Mg–4Ho–0.6Zr alloy. During ageing at 250 °C, the alloy exhibited a strong age hardening response, and the hardness value rose to a maximum value of 83 Hv after 48 h. When 5 wt% Y was added to the Mg–4Ho–0.6Zr alloy, a little increase in hardness was observed in as-quenched condition with a hardness value of 75 Hv, compared with Mg–4Ho–3Y–0.6Zr alloy, and the increment of aging hardness is almost as same as that of Mg–4Ho–3Y–0.6Zr alloy. A further adding the Y from 5 to 7 wt%, the Mg–4Ho–7Y–0.6Zr alloy exhibited a maximum hardness in as-quenched condition and the strongest age hardening response. The hardness values in

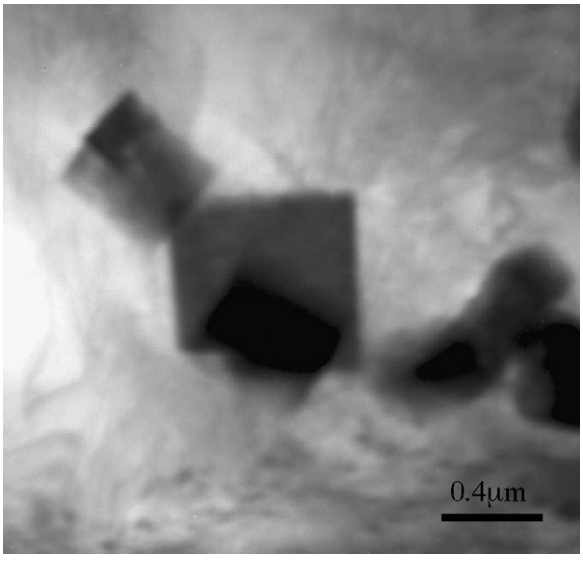

Fig. 3. TEM micrograph of intermetallic particles at grain boundaries in Mg–4Ho–7Y–0.6Zr alloy peak-aged.

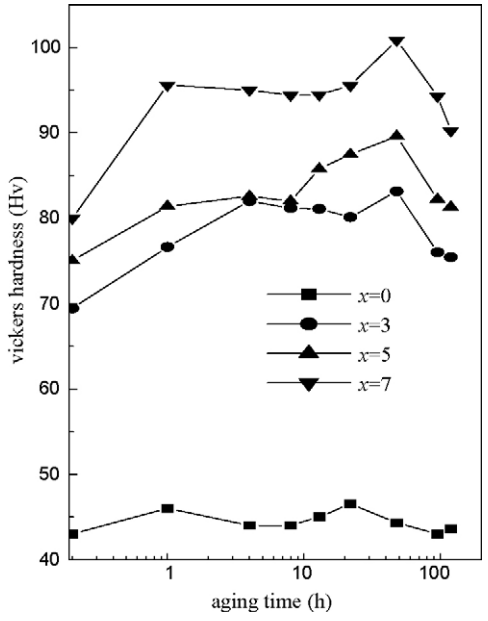

Fig. 4. Aging hardening response at 250 °C of Mg–4Ho-*x*Y–Zr alloys.

the as-quenched and peak-aged conditions were 80 and 100 Hv, respectively.

TEM micrographs of the peak-aged Mg–4Ho–3Y–0.6Zr alloy are shown in Fig. 5. Fine plate-like precipitates and parallel dislocation lines were observed in the interior of the grains. The structure of the plate-like phases was identified by electron diffraction pattern, as shown in Fig. 5(b), to be body-centered cubic (bcc). The precipitates for the alloy seems to be equilibrium β-$Mg_{24}Y(Ho)_5$ phases, as shown in Fig. 5(a). The TEM micrographs of peak-aged Mg–4Ho–7Y–0.6Zr alloy are shown in Fig. 6. Two type precipitates were observed in the interior of the grains. One is the plate-like precipitate shown in Fig. 6(a), with the incident electron beam approximately parallel to [0 0 0 1]α in Fig. 6(b), and this seems to be β′ phase [13]. Another is plate-like precipitate also, which is as same as that of Mg–4Ho–3Y–0.6Zr alloy by EDS. As shown in Fig. 6(d), the density of parallel dislocation lines was increased, compared with that in Fig. 5(c). The parallel dislocation lengths were chiefly hundreds of nanometers and the spacing between them were several ten nanometers. At the same time, many of the dislocations were arranged in networked indicating that considerable recovery had also occurred during cooling to room temperature and tangled with each other, in Fig. 6(e). The average dislocation spacing in the network was measured to be 50–100 nm, indicating higher dislocation density.

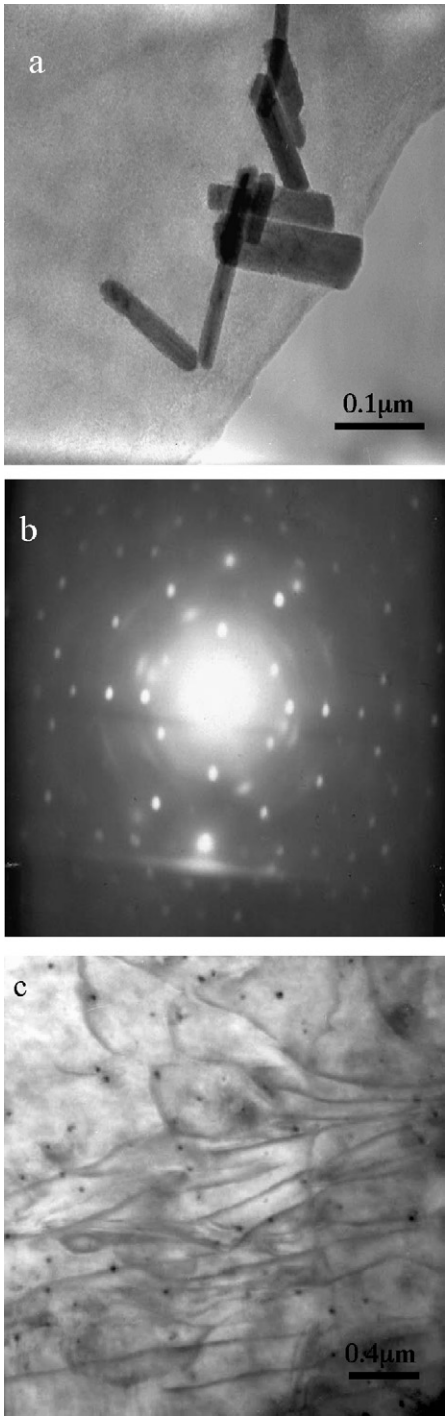

Fig. 5. TEM micrograph of Mg–4Ho–3Y–0.6Zr alloy in peak-aged condition: (a) bright-field images take along [1 1 1] zone axis of β-$Mg_{24}Y(Ho)_5$ phase; (b) [1 1 1] zone axis diffraction pattern from β-$Mg_{24}Y(Ho)_5$ phase; (c) parallel dislocation.

3.2. Tensile properties

Tensile properties of peak-aged samples of Mg–4Ho–0.6Zr, Mg–4Y–3Ho–0.6Zr, Mg–6Y–5Ho–0.6Zr and Mg–6Y–7Ho–0.6Zr alloys are provided in Table 2. At both room temperature and 250 °C, the ultimate tensile strength (UTS), yield strength (YS) and ductility of Mg–4Y–3Ho–0.6Zr alloy were all considerably higher than those of the Y-free alloy. The yield strengths of Mg–4Y–3Ho–0.6Zr alloy were about 110% and 165% higher than those of Y-free alloy at room temperature and 250 °C, respectively. A further increase in the Y content to 5 wt% in the quaternary alloy only led to slightly increase in ultimate tensile strength and yield strength, compared with those of Mg–4Y–3Ho–0.6Zr alloy. When 7 wt% Y was added to the Mg–4Ho–0.6Zr alloy, the alloy exhibited the maximum ultimate tensile strength and yield strength at peak hardness, and the values were 240 and 165 MPa at room temperature, and 204 and 131 MPa at 250 °C, respectively, and the ductility had a remarkable decrease.

3.3. Fractography

Fig. 7 shows SEM images of tensile fracture surface. Fig. 7(a) is the image of Mg–4Y–3Ho–0.6Zr alloy at room temperature. The failure surface was composed of a big tearing ridge running through the image and many dimples. Fig. 7(b) shows the fractography of Mg–6Y–7Ho–0.6Zr alloy at room temperature.

Table 2
Tensile strength of peak-aged samples of Mg–4Ho–xY–0.6Zr alloys (x = 0, 3, 5, and 7 wt%)

Alloy (wt%)	UTS (MPa)		YS (MPa)		Elongation (%)	
	RT	250 °C	RT	250 °C	RT	250 °C
Mg–4Ho–0.6Zr	120	75	62	40	7	16
Mg–4Ho–3Y–0.6Zr	207	174	130	105	11	20
Mg–4Ho–5Y–0.6Zr	215	183	138	112	10	18
Mg–4Ho–7Y–0.6Zr	240	204	165	131	6	12

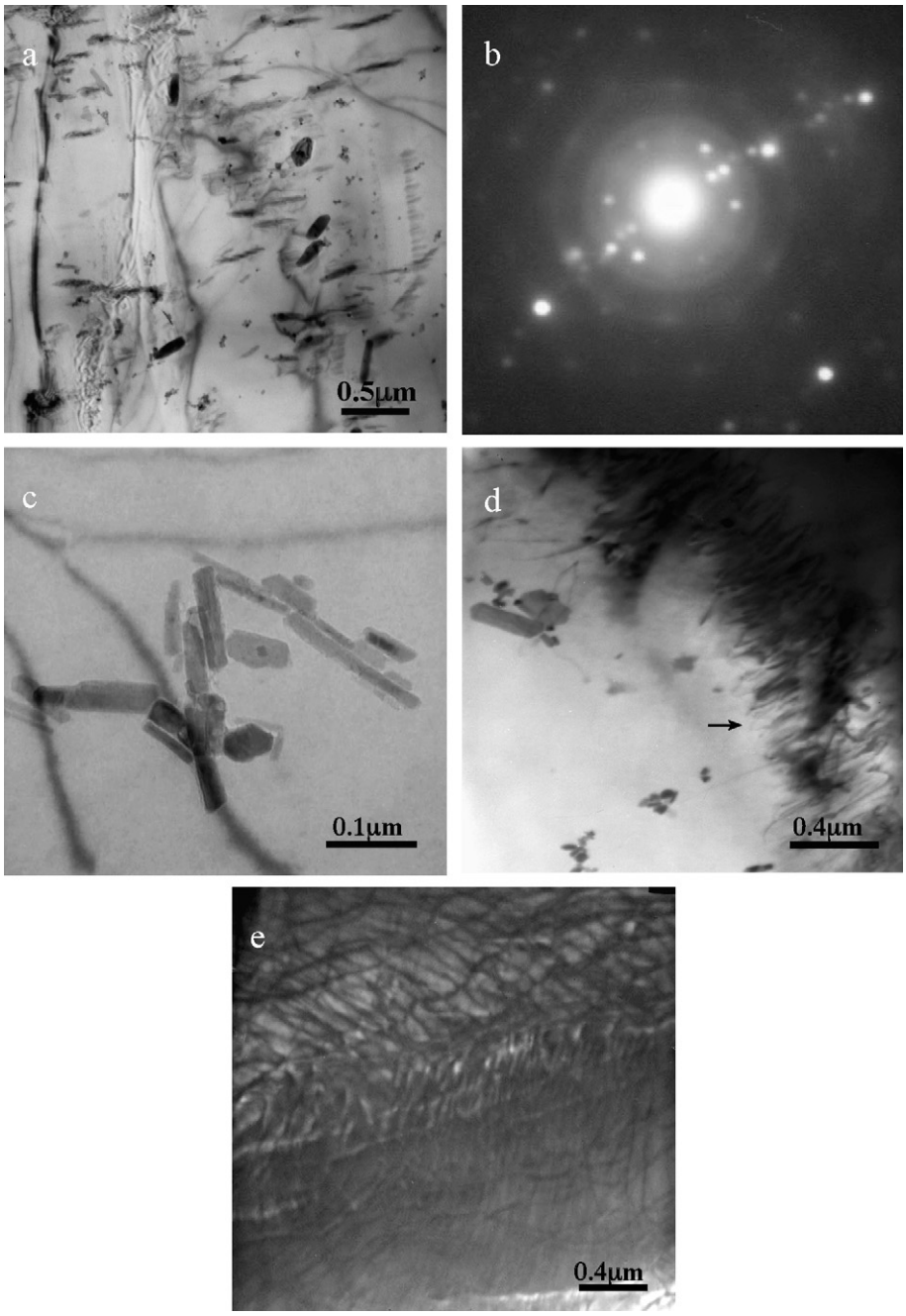

Fig. 6. TEM micrograph of Mg–4Ho–7Y–0.6Zr alloy in peak-aged condition. (a) Distribution of β′ phase beam direction [0 0 0 1]α; (b) the corresponding SAED of (a); (c) distribution of β-$Mg_{24}Y(Ho)_5$ phase; (d) parallel dislocation; (e) dislocation network.

Local areas revealed the typical characteristic of quasi-cleavage and cleavage fracture can be observed which indicated that the fracture surface had a mixed fracture characteristics.

3.4. Discussion

The Mg–4Ho–0.6Zr alloy exhibited an almost negligible age hardening response during isothermal ageing at 250 °C. At 200 °C, the equilibrium solid solubility of Ho in Mg is 2.10 at% (12.8 wt%). Accordingly, almost no precipitates could be observed in the alloy. It was reported that the poor response on ageing of the Mg–6Gd–0.6Zr alloy was attributable to the low fraction and a non-uniform distribution of precipitates [14]. The weak age hardening response of Mg–4Ho–0.6Zr alloy may also associate with Mg–6Gd–0.6Zr alloy.

Addition of Y at level of 3 wt% and above to the Mg–4Ho–0.6Zr alloy resulted in an increase by 60–86% in the as-quenched hardness. The increasing of as-quenched hardness was likely to attribute to the solid solution strengthening. But the increase of density of dislocation was also observed with increasing Y content, as shown in Figs. 5 and 6. Accordingly, it was possible that the remarkable increment in the as-quenched

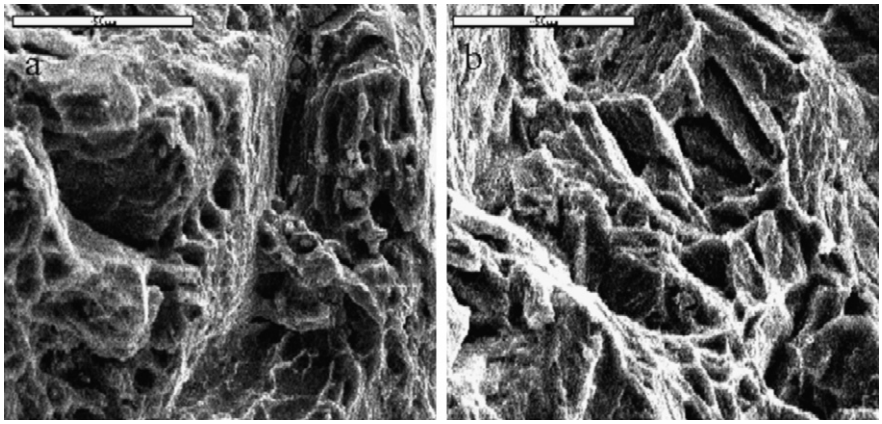

Fig. 7. Fracture surface of the experimental alloys: (a) Mg–3Ho–4Y–0.6Zr alloy; (b) Mg–7Ho–4Y–0.6Zr alloy, tested at room temperature.

hardness was associated with interaction between dislocation and solute atoms.

Addition of Y to Mg–4Ho–0.6Zr alloy can significantly enhance the age hardening response. The remarkable increase of peak hardness appeared to be associated with β-$Mg_{24}Y(Ho)_5$ and/or β′ phases. We considered that the following factor is ascribed to improve the ageing hardening response. The atomic radius of Ho and Y are 1.766 and 1.801 nm, respectively, which confirmed that the crystal lattice of Mg solid solution was disordered when Y was added to the Mg–4Ho–0.6Zr alloy. According, the solid solubility of Ho and Y occurred to change. It was known that the response of ageing proved to be quite little for Mg–4Y and Mg–6Y at high temperature [15]. It was indicated that the solid solubility of Ho and Y would be decreased relatively when Y was added to Mg–4Ho–0.6Zr alloy. According to previous result, Nie and Muddle [16] have reported that the aged-peak microstructure contains predominantly the phases β′, β_1 and β in WE54 alloy. The microstructure of the T6-aged WE43 alloy consisted of both metastable β′ and equilibrium β precipitates [17]. Mg–Gd [11], Mg–Gd–Nd and Mg–Gd–Y alloys [10] exhibits remarkable ageing hardening by precipitation of β″ phase with DO_{19} crystal structure and/or β′ phase with bco crystal structure. In present experiment, the precipitate phase in peak-aged condition in Mg–4Ho–3Y–0.6Zr alloy was different from that in Mg–4Ho–7Y–0.6Zr alloy. Only equilibrium β-$Mg_{24}Y(Ho)_5$ phase was observed in Mg–4Ho–3Y–0.6Zr alloy. It has been reported that the Mg–Gd binary alloy containing less than 10 wt% Gd showed different decomposition without β′ phase [11]. It has also been reported that the β precipitate makes significant contributions to precipitation hardening in Mg–10 wt% Y alloy [18]. Accordingly, it was possible that the equilibrium β-$Mg_{24}Y(Ho)_5$ precipitate was mainly attributed to the improvement of ageing hardening in the Mg–4Ho–0.6Zr alloy. For Mg–4Ho–7Y–0.6Zr alloy, the aged-peak microstructure contains predominantly the phases β′ and β.

The tensile results demonstrated that adding Y to the Mg–4Ho–0.6Zr ternary alloy could improve the mechanical properties, especially improving the stability of the alloy at high temperature (250 °C). According to the TEM observation, it can be confirmed that the precipitate phases occurred change from equilibrium β-$Mg_{24}Y(Ho)_5$ phase to β′ and equilibrium $Mg_{24}Y(Ho)_5$ phases at peak-aged condition with increasing Y content. These β′ and equilibrium β-$Mg_{24}Y(Ho)_5$ phases have high melt point and good thermal stability, which is related with the low diffusion speed of (Y, Ho) elements in the α-Mg matrix. It could be effectively prevent gliding of dislocation and deformation of grain boundaries. It has been reported that the β′ or β phase play a positive role in strengthening by providing effective barriers to gliding dislocation in Mg–Y–Nd alloy [19]. It was known that for Mg alloys containing precipitate particles that are resistant to dislocation shearing, the high strength is associated with microstructure containing a high density of intrinsically strong, plate-shaped precipitates with prismatic habit planes and large aspect ratios, and that precipitate plates formed on habit plane of the matrix phase provide the least effective barrier to gliding dislocations [20]. At the same time, high dense dislocations can also restrain motion of dislocation and growing of grain size. Accordingly, the improvement in strength appeared to be associated with β′ and/or equilibrium β-$Mg_{24}Y(Ho)_5$ precipitates and high density of dislocation.

4. Conclusion

The addition of Y can refine grain of Mg–4Ho–0.6Zr alloy, and the age hardening response of the alloy was improved with increasing Y content significantly. Tensile strength of the alloys increased monotonously with increasing Y content. For Mg–4Ho–7Y–Zr alloy exhibited the maximum ultimate tensile strength and yield strength at peak hardness, and the values were 240 and 165 MPa at room temperature, and 204 and 131 MPa at 250 °C, respectively. The improvement in strength appeared to be associated with β′ and/or equilibrium β-$Mg_{24}Y(Ho)_5$ precipitates and high density of dislocation.

Acknowledgements

This project was supported by Hi-Tech Research and Development Program of China (2006AA03Z520), Chinese Academy of Sciences and Jilin Province.

References

[1] B.L. Mordike, T. Ebert, Mater. Sci. Eng. A 302 (2001) 37–45.
[2] Guangling, St. John David, J. Light Met. 2 (2002) 1–16.
[3] S. Spigarelli, D. Ciccarelli, E. Evangelista, Mater. Lett. 58 (2004) 460–464.
[4] C.J. Ma, M.Q. Liu, G.H. Wu, W.J. Ding, Y.P. Zhu, Mater. Sci. Eng. A 349 (2003) 207–212.
[5] Y.X. Hua, S.K. Guan, X.Q. Zeng, W.J. Ding, Mater. Sci. Eng. A 416 (2006) 109–118.
[6] H.H. Zou, X.Q. Zeng, C.Q. Zhai, W.J. Ding, Mater. Sci. Eng. A 402 (2005) 142–148.
[7] B.L. Morike, Mater. Sci. Eng. A 324 (2002) 103–112.
[8] G.W. Lorimier, Proceedings of the Conference on Magnesium Technology, The institute of Metal London 1987, 1987, pp. 47–53.
[9] I.J. Polmear, Mater. Sci. Technol. 10 (1994) 1–16.
[10] P.J. Aapps, H. Karimzadeh, J.F. King, G.W. Lorimer, Scr. Mater. 48 (2003) 475.
[11] P. Vostry, B. Smola, I. Stulikova, F. von Buch, B.L. Mordike, Phys. Stat. Sol (a) 175 (1999) 491.
[12] P.J. Aapps, H. Karimzadeh, J.F. King, G.W. Lorimer, Phys. Stat. Sol (a) 175 (1999) 1023–1028.
[13] T. Mohri, M. Mabuchi, N. Saito, M. Nakamura, Mater. Sci. Eng. A 257 (1998) 287–294.
[14] J.F. Nie, X. Gao, S.M. Zhu, Scr. Mater. 53 (2005) 1049–1053.
[15] M. Socjusz-Podosek, L. Lity nska, Mater. Chem. Phys. 80 (2003) 472–475.
[16] J.F. Nie, B.C. Muddle, Acta Mater. 48 (2000) 1691–1703.
[17] J.G. Wang, L.M. Hsiung, T.G. Nieh, M. Mabuchi, Mater. Sci. Eng. A 315 (2001) 81–88.
[18] M.X. Zhang, P.M. Kelly, Scr. Mater. 48 (2003) 379–384.
[19] C. Antion, P. Donnadieu, F. Perrard, A. Deschamps, C. Tassin, A. Pisch, Acta Mater. 51 (2003) 5335.
[20] J.F. Nie, Scr. Mater. 48 (2003) 1009–1015.